JCTC Journal of Chemical Theory and Computation

Atomistic Simulation of Adiabatic Reactive Processes Based on Multi-State Potential Energy Surfaces

Jonas Danielsson and Markus Meuwly*

Chemistry Department, University of Basel, Klingelbergstrasse 80, CH-4056 Basel, Switzerland

Received February 28, 2008

Abstract: The adiabatic reactive molecular dynamics (ARMD) method provides a framework to study chemical reactions using molecular dynamics simulations with minimal computational overhead. Here, ARMD is generalized to an arbitrary reactive process between two states in which reactants and products can be treated by an atomistic force field. The implementation is described, and the method is applied to two systems: the kinetics of NO rebinding to myoglobin (Mb) as a validation system and the conformational transition in neuroglobin (Ngb) which explores the full functionality of ARMD. For MbNO, the nonexponential kinetics observed both in experiment and earlier ARMD studies is reproduced. Furthermore, the sensitivity of the results with respect to the asymptotic separation between the two potential energy surfaces (NO bound and unbound) is studied.

1. Introduction

Describing the dynamics of chemical reactions and extracting meaningful information that can be compared with experimental data is a major challenge in computational chemistry. For most chemically and biologically relevant processes the inherent difficulty lies in the large span of time- and length scales involved. Ideally, the computational treatment of chemical reactions in condensed phases, on surfaces, or in macromolecular systems requires methods that are capable of describing motions and time scales in the sub-Å/fs range (electrons, atomic rearrangements) to the tens-of-Å/ms range in a realistic fashion. The computational cost of accurate electronic structure calculations (ab initio calculations including electron correlation) prohibits the direct use of such methods including the time dependence of the process for large systems. On the other hand, the simplified form of the interaction potential used in standard force fields is not designed to describe changes in the electronic structure. The quantum mechanical/molecular mechanical (QM/MM) method[1–4] is a popular way to combine the accuracy of electronic structure calculations for the reacting fragments with the efficiency of classical force fields. This method has been used to locate critical points on the PES, which can provide useful information.[5–7] Typically, studies including dynamics and configurational heterogeneity are carried out at the semiempirical level.[8,9] Exceptions to this are, e.g., proton transfer reactions in small water- and ammonia-containing systems.[10–12] The Empirical Valence Bond (EVB)[13,14] is a method in which the PES is described by two or more valence states, each described parametrized as a force field, which are mixed according to an empirical coupling term. EVB is comparable in efficiency to conventional force field calculations which allows dynamics simulations. In its original version, an EVB representation is calibrated by forcing the calculated ground-state energy at certain points to reproduce their experimentally determined free energies.[13] In more recent applications EVB potentials have also been calibrated in view of data from electronic structure calculations. If the reaction involves a change of electronic state, then surface hopping methods[15,16] where the system can switch between several surfaces in a stochastic process provides a useful way to treat the dynamics. However, computational efficiency is still an issue since the switching probability has to be calculated from nonadiabatic coupling elements, which requires detailed knowledge of the electronic structure. The latter is particularly challenging for systems with a complicated electronic structure, such as metal-containing proteins, where strong multireference character of the metal-center is common.

* Corresponding author e-mail: m.meuwly@unibas.ch.

10.1021/ct800066q CCC: $40.75
Published on Web 06/18/2008

Recently an approach was presented which is applicable to reactions involving two potential energy surfaces where quantum effects (e.g., tunneling or coherence) are less important because the transitions are to a good approximation adiabatic (e.g., due to strong coupling between the two states). Adiabatic Reactive Molecular Dynamics (ARMD) was successfully used to quantitatively study the nonexponential rebinding kinetics of nitric oxide (NO) to myoglobin (Mb).[17] Photolysis and subsequent rebinding of small molecules to the heme group of globular proteins such as myoglobin and hemoglobin has become one of the paradigm processes in biophysics and has provided a substantial insight into the interplay between structure, function, and dynamics of protein−ligand complexes.[18,19] Earlier experiments of myoglobin rebinding kinetics focused on the binding of CO vs O_2.[20–22] Given the important biological role of NO as a messenger molecule involved in platelet aggregation and immune response,[23,24] the interest in the reactive dynamics between NO and Mb has considerably increased.[25–29] Finally, MbNO is also an interesting system for ultrafast spectroscopy given its rapid rebinding kinetics with a fast time scale in the picosecond range[28,30] and for molecular dynamics simulations,[17,27] since many interesting processes occur on a time scale suitable for computational work.

Neuroglobin is a recently discovered member of the globin protein family expressed in the nerve cells of vertebrates.[31] The function of this protein is unknown, although it seems to be upregulated in cases of hypoxia (oxygen deficiency), suggesting a protective role.[32] The crystal structure of unligated neuroglobin was recently solved and revealed a number of interesting differences compared to other globins.[33] Unlike myoglobin, the unligated protein is hexacoordinated, with active-site histidines acting as axial ligands. Analysis of the X-ray experiments found that the measured electron density in the active site could not be well fitted with a single conformation. Using a second conformation with 30% occupancy and a different heme orientation the quality of the fitting was considerably improved. The biological significance for these almost degenerate conformations is unknown, although NMR experiments indicate that binding of CN^- is significantly slower in one of the conformations.[34]

In the present work the general formulation of ARMD to treat reactions involving two potential energy surfaces is presented and applied to two system of biological interest. First the Mb-NO rebinding problem[27,28] is reconsidered to validate the generalized implementation, and second we study the equilibrium and switching between different conformational states in neuroglobin[33] to demonstrate the generality of the code and also show how one can parametrize the method from experimental data. The current work is structured as follows. First, details about the ARMD algorithm and its implementation are provided. Next, the computational setup for the two test systems is described, and the results from extensive ARMD simulations are presented. Finally, conclusions summarize the work.

2. Computational Methods.

2.1. The ARMD Algorithm. In the following, the potential energy surfaces (PESs) considered have the standard CHARMM[35] form

$$\begin{aligned}\vec{V(x)} = &\sum_{bonds}\frac{k_i}{2}(r_i-r_i^0)^2+\sum_{angles}\frac{k_j}{2}(\theta_j-\theta_j^0)^2+\\ &\sum_{dihedrals}\sum_{m=1}^{mmax}k_k^m\cos(m\varphi_k-\gamma_k)+\\ &\sum_{impropers}\frac{k_l}{2}(\phi_l-\phi_l^0)^2+\\ &\sum_{i<j}\frac{q_iq_j}{4\pi\varepsilon 0 r_{ij}}+4\varepsilon_{ij}\left[\left(\frac{\sigma_{ij}}{r_{ij}}\right)^{12}-\left(\frac{\sigma_{ij}}{r_{ij}}\right)^{6}\right]\end{aligned} \quad (1)$$

where r_i, θ_j, ϕ_k, and φ_l are bond lengths, covalent angles, dihedrals, and improper dihedrals, respectively, the k_x parameters are force constants, γ_k is a dihedral offset, q_i are atomic partial charges, and σ_{ij}, ε_{ij} are pairwise Lennard-Jones radius and well-depths. In addition to these terms, Morse potentials are used for anharmonic bonds

$$V_{Morse} = D_e(1-\exp(-\beta(r-r_0)))^2 \quad (2)$$

where r_0 is the equilibrium bond length, D_e is the dissociation energy, and β is the anharmonicity parameter. V_{Morse} is particularly useful in studying the breaking and formation of bonds.

The force field description (eq 1) of the reactants (V_R) and the products (V_P) differs by a number of force field parameters. In a macromolecular system the number of energy terms by which V_R and V_P differ is usually small compared to the total number of energy terms. The latter is of order N for bonded and of order N^2 for nonbonded terms, where N is the total number of atoms. Thus, it is only necessary to provide a small number of additional parameters compared to a standard simulation to describe the differences between R and P.

For the general case where V_R and V_P represent different electronic states, the two PESs are separated by an asymptotic energy difference that does not appear in a classical force field. In standard force fields only energy differences have physical significance, whereas the absolute energy scale is unimportant. For a meaningful comparison of the energies of the two force fields defining V_R and V_P, a constant Δ (the "asymptotic separation") is introduced so that $V_R+\Delta$ and V_P share a common 'zero' of energy. In principle, the energy difference between two electronic states at a chosen geometry can be estimated from a single quantum chemical calculation, which allows to set Δ. In practice, however, it is preferable to calibrate Δ to reproduce experimental data.

The dynamics of the system is initiated and propagated on the ground state $V_0(\vec{x}) = \min[V_R+\Delta, V_P]$. At each time step the energy difference $\Delta V = V_R - V_P + \Delta$ is calculated and compared with the previous step. If ΔV switches sign at time t_{cross}, a crossing between the PESs has been detected. Since prior to the crossing point the dynamics takes place on one diabatic surface, the mixing of surfaces due to coupling has to be introduced a posteriori to create the adiabatic surface. This is achieved by reconstructing the system at the time point $t_{cross} - T_{mix}/2$. The crossing between

the two diabatic surfaces is then carried out by gradually switching the PES from $V_R + \Delta$ to V_P by using a time dependent switching function $f(t)$ according to

$$V = f(t)(V_R + \Delta) + (1 - f(t))V_P \quad (3)$$

$f(t)$ is chosen so that at the crossing time t_{cross} the surfaces are mixed with equal contributions, i.e $f(t_{cross}) = 0.5$. In this way the procedure is time reversible in the sense that a backward trajectory will follow the same path. Furthermore $0 \le f(t) \le 1$ and $f(t)$ increases monotonically with t. Among the possible functions that fulfill these conditions the following was deemed suitable

$$f(t) = \frac{1}{2}[\tanh(\alpha(t - t_{cross})/(T_{mix} - \delta t)) + 1] \quad (4)$$

here written for a switch from V_P to V_R. The constant α is chosen so that $f(t)$ is close to 0 and 1 for $0 < t < t_{cross} - T_{mix}/2$ and $t > t_{cross} + T_{mix}/2$, respectively. In the present simulations $\alpha = 4.8$ was used. In the opposite switch process, $f(t)$ is replaced with $1 - f(t)$. After the switch the dynamics continues on V_P. During the switch and for a time interval $t = T_{mix}/2$ after a crossing, no new crossing can take place. This avoids that two crossings overlap in time. For $t > T_{mix}/2$ the algorithm is reset, ΔV is monitored, and configurations are stored for a next surface crossing.

2.2. Implementation and User Interface. The strategy outlined above was implemented in CHARMM together with a user interface designed to make the method as general and flexible as possible. For details concerning conventions used in CHARMM the original reference should be consulted.[35] The input data required are the parameters Δ, T_{mix}, and α and all force field parameters that differ between V_R and V_P. If the atom connectivities for the system in V_R and V_P differ (i.e., a chemical reaction is investigated) the exclusion lists controlling the nonbonded interactions between atoms separated by two or three covalent bonds in the two states have to be modified. Such modifications are automatically generated from the protein structure file and the additional input concerning the changes in topology between the two surfaces.

Energy terms that differ between V_R and V_P are modified according to $f(t)(V_R+\Delta) + (1-f(t))V_P$ term by term in eq 1 during a surface crossing. However, for the electrostatic interaction, instead of scaling the Coulombic energy term, the charges q_i which change between V_R and V_P are scaled: $q_i(t) = f(t)q_i^{(R)} + (1-f(t))q_i^{(P)}$, and then the electrostatic energy and forces can be calculated by any available method. This simplifies the use of different techniques such as shifted cutoff, reaction fields,[36] or Ewald summation[37] for treating the long-range electrostatics. Note that this leads to a quadratic scaling of electrostatic interaction terms between pairs of atoms where both charges are subject to change during the switch.

2.3. Simulation Setup and Protocols. All simulations were carried out using CHARMM[35] together with the CROSS module described above. Except for the parameters used for the reacting regions (see further below) all parameters are from the CHARMM22[38] all-atom force field. For water molecules the TIP3P model was used.[39]

For both systems (rebinding of NO to myoglobin and conformational substates in Ngb) stochastic boundary conditions[40] were used. The water sphere (radius of 25 Å) was centered around the iron atom of the heme group, and the radius of the inner region where free Newtonian dynamics takes place was 20 Å. The systems were solvated by overlaying the protein with a pre-equilibrated water sphere and removing all waters in close contact (<2.8 Å) with any atom of the protein. The water sphere was rotated, and the overlay was repeated twice. For all simulations the SHAKE[41] algorithm was applied to all covalently bound hydrogen atoms which allows a time step of 1 fs.

Table 1. Parameters of the Two Surfaces Used in the Neuroglobin Simulations

parameter	surface 1 (70%)	surface 2 (30%)
r_0/Å (His64(N_ε)-Fe)	2.40	1.85
k_b/kcal·mol^{-1}·Å^{-2} (His64(N_ε)-Fe)	50.0	50.0
r_0/Å (His96(N_ε -Fe))	1.90	2.00
k_b/kcal·mol^{-1}·Å^{-2} (His96(N_ε)-Fe)	75.0	75.0
θ_0/° (His64(N_ε)-Fe-N_{Heme})	87.00	80.00
k_a/kcal·mol^{-1}·rad^{-2} (His64(N_ε)-Fe-N_{Heme})	50.00	40.00
θ_0/° (His96(N_ε)-Fe-N_{Heme})	93.00	100.00
k_a/kcal·mol^{-1}·rad^{-2} (His96(N_ε)-Fe-N_{Heme})	50.00	40.00
θ_0/° (His64(N_ε)-Fe-His96(N_ε))	177.00	150.00
k_a/kcal·mol^{-1}·rad^{-2} (His64(N_ε)-Fe-His96(N_ε))	50.00	60.00
ϕ_0/° (His64/96(C_δ)-His64/96(N_ε)-Fe-N_{Heme})	0.00	0.00
k_d/kcal·mol^{-1}·rad^{-2} (His64/96(C_δ)-His64/96(N_ε)-Fe-N_{Heme})	0.05	0.05
m (His64/96(C_δ)-His64/96(N_ε)-Fe-N $_{Heme}$)	4	4

Rebinding in MbNO. The initial coordinates for MbNO were taken from the previous study of Nutt and Meuwly,[17] to allow direct comparison. These initial conditions represent a state where the ligand has been photodissociated from the heme group after equilibration in the bound state. The velocities are then randomized by sampling from the appropriate Maxwell−Boltzmann distribution. Subsequently, statistics on the rebinding events is collected as described previously.[17] The experimentally accessible observable is the fraction $N(t)$ of unbound ligand survived. In ARMD this corresponds to the fraction of trajectories still on the unbound PES at time t after photodissociation. The force field parameters for the 5- and 6-coordinated heme group were taken from Meuwly et al.[27] The NO was represented by a simple two-center charge model with charges $-qO = qN = 0.063e$ and a harmonic oscillator as internal potential energy function. In the previous ARMD study of this system[17] a two-dimensional PES from extensive QM calculations was used with the ligand center-of-mass (CoM) to iron distance and the Fe−CoM−O angle as the coordinates.[29] For the current validation simulations the force field described in previous work was used for the bound state, namely a Morse oscillator for the ligand-heme coordination bond, and a harmonic term for the Fe−N−O angle.[27] The simpler PES for the Fe-NO interaction was used to test ARMD under common conditions where no specialized interaction potentials for specific coordinates are available. Also, it is of interest to see whether the salient features of the rebinding reaction can be understood without a more sophisticated PES.

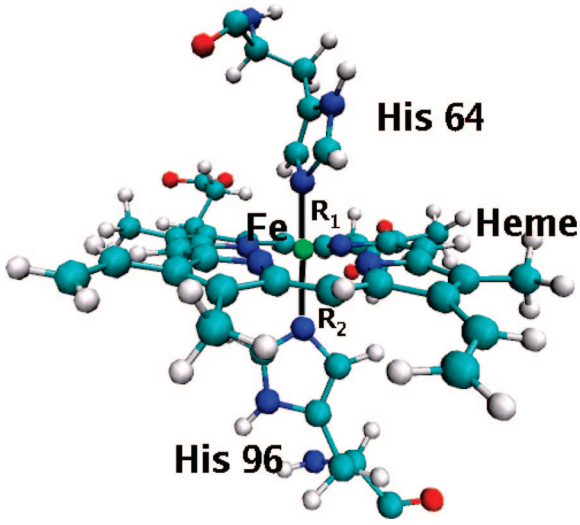

Figure 1. Active site of neuroglobin with the two coordinating histidines (64 and 96), the heme group with the central Fe atom (green), and the two Fe−N distances R_1 and R_2 used to define the reaction coordinate R_u in the umbrella sampling calculations.

Conformational Substates in Ngb. In the experimental structure of neuroglobin two conformations with relative populations 70/30 were observed.[33] The heme group remains hexacoordinated in both cases, but the orientation and bond lengths between the ferric heme iron and the two coordinating histidine groups differ. Switching between these two states can therefore be regarded as a bound-to-bound transition. The force field parameters (see Table 1) for the two observed conformations of neuroglobin were derived from the experimentally observed geometries in combination with standard force constants adapted from similar systems.

The initial structure for Ngb was the wild-type, ligand-free structure (PDB accession code 1Q1F). Minimization and equilibration of the protein were carried out individually on both surfaces by adjusting the Δ parameter to large positive or negative values which avoids crossings between the two states. The resulting average potential energies can be used to estimate Δ such that a certain relative energy between the two stable forms are obtained. Longer simulations of 500 ps each were used to explore the relative population of the two surfaces for different separations Δ between the two PESs. From these preliminary simulations, an approximate progression coordinate can be constructed which is a useful guide for more detailed sampling methods, such as umbrella sampling. This procedure was used in neuroglobin along the coordinate R_u defined by the ratio R_1/R_2 where R_1 and R_2 are shown in Figure 1. A single window with a harmonic umbrella potential was sufficient to obtain good sampling along the entire relevant range of R_u ε (0.8−1.2). The umbrella potential was centered at $R_u = 0.93$, which corresponds approximately to the transition state, and a force constant of 40 kcal/mol was used. From these simulations, reliable estimates of the free energy profile and relative population of the two states can be calculated.

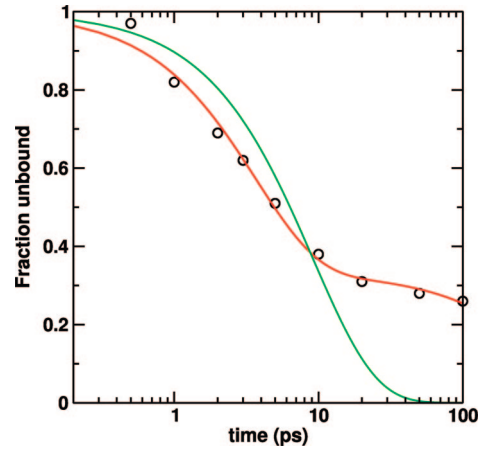

Figure 2. Fraction of unbound trajectories in photodissociated MbNO as a function of time (logarithmic scale) after photodissociation (black circles) for Δ = 65 kcal/mol, together with a double exponential (red) and the best single exponential fit (green).

3. Results and Discussion

3.1. Validation of the Implementation: MbNO as a Test Case. Experimental work on the rebinding kinetics has shown that the rebinding reaction after photodissociation of MbNO is nonexponential in time.[25,28] For a geminate rebinding process, $N(t)$ follows an exponential decay with a single time constant τ and a corresponding rate constant $\lambda = \tau^{-1}$ according to

$$N(t) = e^{-t/\tau} \tag{5}$$

For cases where such a decay law does not reproduce the data, either a time-dependent rate constant $\tau(t)$ (which gives rise to a so-called stretched exponential decay)[42] is used or an ansatz as a sum of i exponentials

$$N(t) = \sum_i w_i e^{-t/\tau_i} \quad \sum_i w_i = 1 \tag{6}$$

with weights w_i is assumed. The generalization of this expression for continuous rate distributions $g(\lambda)$ leads to

$$N(t) = \int g(\lambda) e^{-\lambda t} d\lambda \tag{7}$$

From a number N_{traj} of ARMD trajectories with initial conditions that represent the ensemble of ligands after photodissociation, $N(t)$ can then be approximated by the expression

$$N(t) = \frac{1}{N_{traj}} \sum_{j=1}^{N_{traj}} H(t - t_{cross}^{(j)}) \tag{8}$$

where $H(t)$ is the Heaviside function, and $t_{cross}^{(j)}$ is the observed crossing time for trajectory j. For the present validation $N_{traj} = 150$, which is considerably less than in the original study of Nutt and Meuwly where $N_{traj} = 6000$. However, it is still sufficient to distinguish between exponential and nonexponential rebinding kinetics.

The function $N(t)$ from the present simulations is shown in Figure 2. The survival fraction has a nonexponential time dependence. A single exponential decay (green) does not provide a meaningful fit, particularly not for the long time

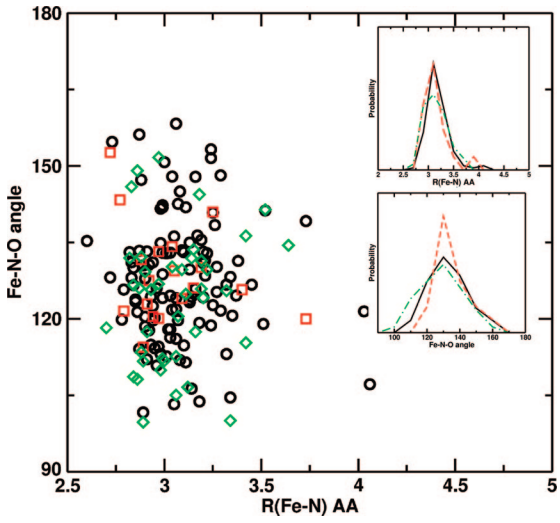

Figure 3. The crossing geometries of NO rebinding to Mb with 3 different values of Δ (red squares Δ = 60, black circles Δ = 65, and green diamonds Δ = 70 kcal/mol) projected onto the distance between iron and the nitrogen of the ligand R_{FeN} and the angle between iron and the NO ligand θ_{FeNO}. The insets show the distributions of crossing points along the R_{FeN} (upper) and θ_{FeNO} (lower) coordinates. For the insets, broken, solid, and dash-dotted lines denote Δ = 60, 65, and 70 kcal/mol, respectively.

behavior. If a double exponential is used, then the data can be fit over the entire time range. The two time constants are $\tau_1 = 3.6$ ps and $\tau_2 = 373$ ps, although τ_2 is not well defined and the uncertainty associated with it is quite large, given that only 8 recrossing events are observed with $t_{cross} > 20$ ps. The fast and slow components have weights of $w_1 = 0.66$ and $w_2 = 0.34$, respectively. Experimentally, ultrafast IR spectroscopy results could be fitted to a double exponential with time constants 5.3 and 133 ps and weights of 0.54 and 0.46 for the disappearance of the free NO stretch mode after photolysis.[25,28] The earlier computational study gave time constants $\tau_1 = 3.1$ ps and $\tau_2 = 18.9$ ps, but there a considerably more complex PES was used for both, the unbound ligand (a 3 point charge model and a Morse potential to describe the NO stretch) and the bound state (a two-dimensional PES based on extensive DFT calculations), that allowed for rebinding both in the Fe-NO and Fe-ON orientation.[17,29]

To visualize the crossing seam all observed crossing geometries are projected onto a plane containing the iron nitrogen distance *RFe-N* and the angle formed by the iron and the ligand *θFe-NO* (see Figure 3, black circles). As in the previous study the most probable iron-ligand separation *RFe-N* lies between 3.0 Å and 3.1 Å, but values as large as 4.05 Å occur. The distribution of *θFe-NO* is centered around 127° with a width of ≈50°. Figure 3 establishes that the transition between the bound and the unbound state is not a single point in phase space but rather an ensemble of structures. Furthermore, it is clear that *RFe-N* and *θFe-NO* alone will not provide a good description of the crossing manifold but that the crossing geometry is also modulated by additional environmental degrees of freedom.

The influence of the asymptotic separation Δ on the observed kinetics is summarized in Figure 4 where $N(t)$ is

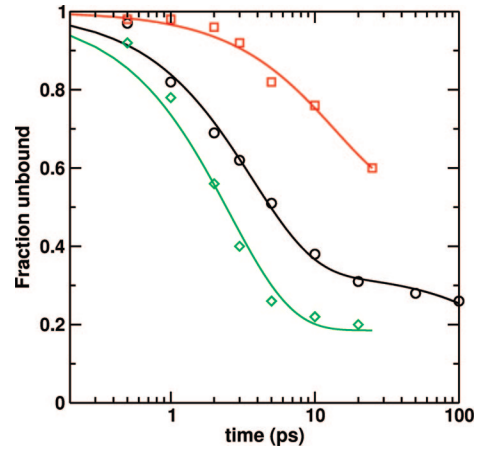

Figure 4. Rebinding curves for the MbNO system calculated as in Figure 2 with three different values of Δ (red squares Δ = 60, black circles Δ = 65, and green diamonds Δ = 70 kcal/mol). The solid lines in respective color represent double exponential fits to the simulated data.

reported for values of Δ 5 kcal/mol higher and lower than the one chosen above (65 kcal/mol). For these calculations a smaller number $N_{traj} = 50$ of reactive trajectories was used, and the maximum trajectory length was 25 ps. As found previously,[17] the choice of Δ has a marked influence on the observed time scales. However, the existence of two rebinding time scales is independent of the value for Δ. Because the time scale of the present simulations does not fully describe the longer decay constant only the fast time scale τ_1 is analyzed in more detail. The constants τ_1 are 2.6, 3.6, and 13.8 ps for Δ = 70, 65, and 60 kcal/mol, respectively. This reflects an increase of the rebinding barrier (the so-called "inner barrier") with decreasing Δ. It is also instructive to consider the weights w_1 as Δ decreases. They decrease from 0.81 to 0.48. Again, this is a manifestation of the importance of the inner barrier which determines the fast rebinding rate.

The value of Δ not only influences the barrier of the reaction but also potentially changes the ensemble that determines the crossing seam. To investigate the sensitivity of the crossing geometries on Δ the crossing geometries were projected as described above for the different values of Δ (Figure 3). For the current system, the crossing manifold is found to be largely insensitive to the value of Δ which, however, may be different for other applications. For the distributions or *RFe-N* no effect can be seen, whereas a weak trend toward a larger average and smaller spread of $\theta_{Fe\text{-}NO}$ can be seen (124° with Δ = 70 kcal/mol to 129° with Δ = 60 kcal/mol).

It is also of interest to consider the dependence on the mixing time T_{mix}. To this end, constant-energy (*NVE*) simulations have been performed, and the total energy was followed as a function of T_{mix}. For very short T_{mix} (≤5 fs), an irregular change of the total energy is observed. This limit represents an abrupt change of the PES during the crossing. The T_{mix} that minimizes the total energy change (≤1 kcal/mol, i.e. "chemical accuracy") for the system studied here is around 10 fs. With increasing T_{mix}, the error in total energy increases during the crossing which is due to the longer time

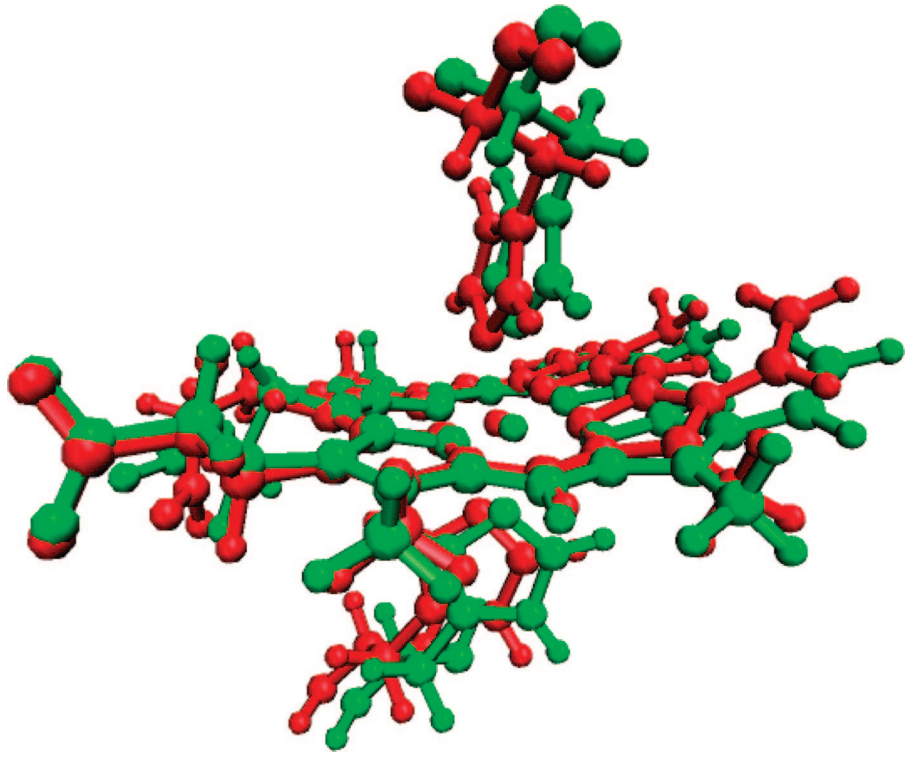

Figure 5. Comparison of the active site structure in neuroglobin for the lower populated state p_2 (red) and the state with higher population p_1 (green). The picture shows the heme group and the two coordinating histidines His64 (above the heme) and His96 (below the heme).

the system spends in the crossing region during the switching. However, even with switching times up to 30 fs, the error is less than 2 kcal/mol which is much smaller than the fluctuations for simulations in the canonical ensemble, which is the usual mode in which ARMD simulations are run. The optimal mixing times found here are comparable to those reported for nonadiabatic reactions using the Coherent Switching with Decay of Mixing (CSDM) which was developed for small molecular systems.[43,44]

Recently, a multidimensional PES for CO-bound and free Mb was presented which includes the effect of spin−orbit interactions.[45] The 6-dimensional PES was fitted to ground-state ab initio energies and the gaps between the ground and the electronically excited states. However, until now, the PESs were not used in dynamics simulations, and, thus, their validity in view of the experimental results (energetics, infrared spectroscopy, rebinding dynamics) for either of the states (bound and unbound) cannot be judged.

3.2. Conformational Equilibrium in Ngb. A more general application of ARMD is the investigation of the equilibrium between two conformational states in Ngb (see Figure 5). In this case at least one of all common bonded force field terms (bonds, angles, and dihedral angles) change between the two states in question. Experimentally, the relative populations and the geometrical features of the conformations involved have been characterized.[33] Furthermore, the two conformational substates are likely to be of biological relevance (allosteric control), which further motivates its understanding with the generalized ARMD procedure. To study the conformational equilibrium, the two states were treated with separate potential energy surfaces. Table 1 summarizes the parameters used for these simulations. This is mainly a convenient way to represent a conformational transition between two well-defined states on a complex potential energy surface. However, the conformational change itself does not involve an electronic transition between two states. This example also serves as an illustration of how Δ can be calibrated from experimental data.

The experimental information available about these two conformational substates is their structures and their relative population (70% and 30%).[33] Consequently, Δ is chosen such as to reproduce the correct occupation of the two states: substate 1 (characterized by PES 1) with 70% population and substate 2 (characterized by PES 2) with 30% population. These two PESs only differ in the force field parameters to correctly describe the experimentally determined structures of substates 1 and 2.

Exploratory simulations showed that the barrier for the conformational change is sufficiently high to make it a "rare" event: typically several hundreds of picoseconds pass between transitions. Thus, the direct sampling of the conformational change and determination of Δ is computationally demanding. To better characterize the transitions, umbrella sampling[46] was chosen as a method to guide the system toward the crossing seam. The progression coordinate, $R_u = R_1/R_2$, was chosen such as to separate the two PESs and still be restricted to a finite interval so that a single harmonic umbrella potential could be used to increase sampling over this interval. Figure 6 shows that $R_u(t)$ switches between two stable positions at 0.85 and 1.01. The switches between these are almost perfectly correlated in time with the crossings as seen from the time series of the energy difference between the two conformational states. It can also

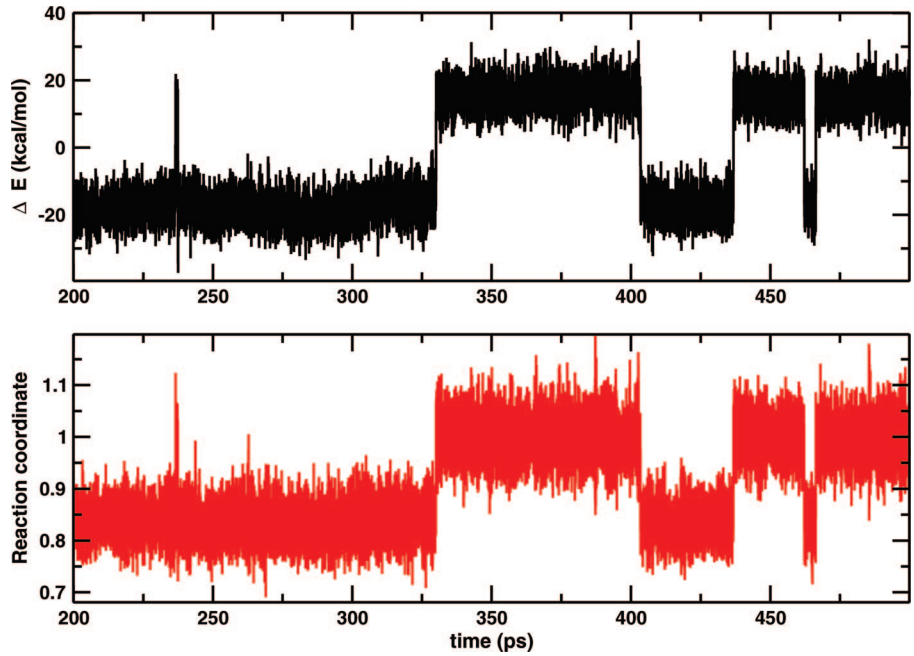

Figure 6. Comparison of the time series for the energy difference $\Delta E = V_1 - V_2$ (above) and the umbrella coordinate R_u (below) defined in the text for the conformational transition in neuroglobin. The correlation between ΔE and the switching of R_u is evident.

be seen in Figure 6 that although R_u clearly can be used to separate the two states, there is a small range around $R_u \approx 0.95$ which is sampled regardless of which state the system is in. Thus, no simple single coordinate can fully describe the transition between the two manifolds, since the energy difference ΔE is also modulated by collective coordinates of the environment, leading to e.g fluctuations of the electrostatic field.

A suitable center for the umbrella potential was determined from a simulation which sampled the conformational transition (see Figure 6) and provided $R_u = 0.93$. Applying the umbrella potential increases the number of transitions from which meaningful statistics for the populations p_1 and p_2 can be estimated. From experiment, the ratio $p_1/p_2 = 70/30$ was determined.[33] The following two-state model is useful to describe the population p_1 as a function of the free energy difference between states 1 and 2. If the free energy difference between the two surfaces at $\Delta = 0$ is $\Delta G(\Delta{=}0) \equiv G = G_1 - G_2$ and the zero of the free energy is assumed for PES 2 ($G_2{=}0$), then the following expression describes the population p_1 on surface 1

$$p_1 = \frac{\exp(-\beta(G+\Delta))}{1+\exp(-\beta(G+\Delta))} = \frac{1}{1+\exp(\beta(G+\Delta))} \quad (9)$$

Thus, a relative population of 70/30 corresponds to a free energy difference of -1.4 kcal/mol between the two states at $T = 300$ K.

The value of Δ was calibrated as follows. Energy minimizations on the two surfaces V_1 and V_2 give an estimate for the (conformationally unaveraged) energy difference $V_1 - V_2 = 4.8$ kcal/mol, which has the wrong sign compared to experiment. To match $V_1 - V_2 + \Delta$ with the estimated free energy difference from experiment $\Delta = -6.2$ kcal/mol was chosen. Next, short umbrella sampling runs starting from each surface were run which suggested that $\Delta = -6.2$ kcal/mol was too low (trajectories initiated on V_2 cross in less than 1 ps and never cross back). To find a range where an equilibrium could be simulated, Δ values between -3.0 and -4.5 kcal/mol were chosen. Five 500 ps simulations with Δ values of -3.0, -3.3, -3.6, -3.9, and -4.2 kcal/mol were run, each with a harmonic umbrella centered at $R_u = 0.93$ and a force constant of 40 kcal/mol. The population of p_1 for each Δ is plotted in Figure 7 and can be represented by eq 9. However, the data from the simulations contain statistical uncertainty, because only ≈10 crossings occur during each 500 ps trajectory. To better characterize the

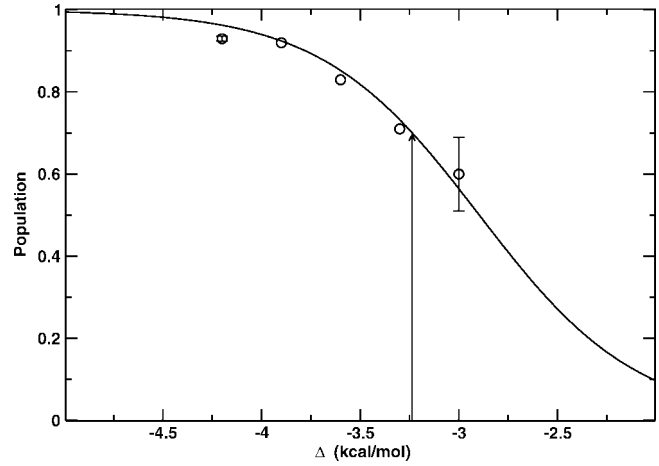

Figure 7. Calculated population of V_1 from umbrella sampling simulations as a function of Δ (circles) and a fit based on the two-state statistical model (solid line). The error bars for $\Delta = -3.0$ and -4.2 kcal/mol are based on the standard deviation from 5 independent simulations. The experimentally observed population $p_1 = 0.7$ is marked by an arrow.

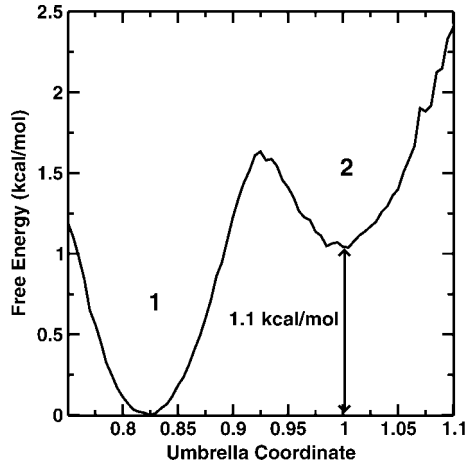

Figure 8. Free energy profile along R_u in neuroglobin from umbrella sampling calculations with $\Delta = -3.3$ kcal/mol. The higher energy state 2 is destabilized by 1.1 kcal/mol relative to the more stable state 1. The forward barrier 1→2 is 1.6 kcal/mol compared to a reverse barrier 2 → 1 of 0.5 kcal/mol.

populations, error bars for $\Delta = -3.0$ and -4.2 kcal/mol were determined from 5 independent simulations of 500 ps each (see Figure 7).

Fitting the simulated data to eq 9 at $T = 300$ K provides an analytical expression for $p_1(\Delta)$. The only free parameter in eq 9 is the free energy difference G at $\Delta = 0$ kcal/mol, which gives $G = 2.9$ kcal/mol. From the fitted curve $\Delta \approx -3.3$ kcal/mol reproduces the experimentally observed population $p_1 = 0.7$. To improve the statistics, the trajectory with $\Delta = -3.3$ kcal/mol was continued for another 500 ps leading to a total of 22 crossings, and the data were used to calculate a free energy profile $G(R_u)$, shown in Figure 8. The free energy difference $\Delta G = 1.1 \pm 0.25$ kcal/mol between the two minima is in quite good agreement with that derived from experiment ($\Delta G = 1.4$ kcal/mol). The error in ΔG is estimated from the error bar of $p(1)$ for $\Delta = 3.0$ kcal/mol (Figure 7). The estimated asymptotic separation $\Delta = 3.3$ kcal/mol could be used in further studies of Ngb to investigate e.g different mutants and their influence on the equilibrium between these two states.

4. Conclusions

The present work has generalized and presented in detail Adiabatic Reactive Molecular Dynamics for studying reactive processes and transitions between potential energy surfaces in large systems where quantum effects are not dominant (adiabatic reactions) or even absent (conformational transition where conformers can be described by different force fields). The implementation was applied to bond breaking/bond formation processes and conformational transitions, and a user interface handles the necessary input. Two parameters (Δ and T_{mix}) set by the user define the method, and the influence of these was analyzed. By applying the method to two realistic and different test cases (myoglobin and neuroglobin) the generality was demonstrated and possible procedures to calibrate the parameters were discussed. Furthermore, ARMD interfaces with most sampling enhancing methods such as targeted MD,[47] metadynamics,[48] replica exchange MD,[49] or umbrella sampling.[46] The latter was used here to investigate the transitions between two conformational substates in neuroglobin, where the barrier between the two states was significantly above the thermal energy.

As a validation for the general ARMD method the rebinding of NO to Mb was considered. The results from the simulations of Mb-NO show that the nonexponential kinetics of ligand rebinding after photodissociation is also observed using the generalized version of ARMD, as was the case with the dedicated implementation.[17] It was found that the fast phase kinetics is controlled by the parameter Δ which determines the inner barrier. The crossing seam is quite similar as the one observed in the earlier study[17] and does not change appreciably for different values of Δ.

The application of ARMD to the conformational equilibrium in neuroglobin establishes that the method can be successfully applied to general reactions where an arbitrary number of force field terms (see eq 1) can be created, deleted, or modified. It was demonstrated how a computational scan of the parameter Δ in combination with a simple two-state model can be used to calibrate ARMD in view of experimental data. This opens the possibility to characterize the reaction at an atomistic level and provides insight which is complementary to experimental investigations.

It is of interest to discuss ARMD in the light of other methods proposed to study reactive processes. An approach related to the one presented here was applied to the rebinding of NO in myoglobin.[50] This work considered a model where the reaction progresses along the Fe−N*NO* separation ρ. To describe the transition between the bound and the unbound state, a switching function depending on ρ was employed. With this approach the correct trends for the picosecond recombination in different Mb mutants at position 29 could be reproduced. A disadvantage is that the approach relies on a geometrical definition of the progression coordinate. It is known that only in the simplest systems (e.g., some proton transfer reactions) a meaningful progression coordinate can be guessed. In more complex systems the relevant coordinates are less obvious, and different choices can lead to different results, as was shown for the isomerization of a tyrosine ring in the bovine pancreatic trypsin inhibitor.[51] Instead of the explicit definition of a (potentially unsuitable) progression coordinate, ARMD performs the switching in time. This opens the possibility to use ARMD to determine suitable progression coordinates a posteriori from the motions between reactants and products.

An alternative procedure employs a Hamiltonian which interpolates between the bound and the unbound system.[52] From a long MD simulation transition state configurations are approximately located, further relaxed (quenched) by minimization, and either end up in the product or the reactant well. From several hundred simulations of unbound Mb-CO the distribution of barrier heights at different temperatures was determined, and results for the width and peak position of the distribution were found to be in qualitative agreement with experiment. Because the approach is primarily based on relaxing the transition state structures it is not clear how to calculate dynamical properties from it. Also, the effect of

the surrounding solvent is difficult to account for explicitly with this approach. In fact, the simulations were carried out with implicit solvent.

It is also of interest to briefly discuss similarities and differences between ARMD and EVB/EVB-like approaches. Both methods try to combine the speed of molecular dynamics simulations with added functionality in a force field description of the total energy of a system. Both methods are parametrized and parameter optimization may be a lengthy and arduous process, and their determination is preferably done with respect to experimental data. The starting point for ARMD is that the interactions and dynamics in the reactant (R) and product (P) states of a molecular system can be characterized in a meaningful way using force fields and atomistic simulations. For this, observables (which may be different for R and P) for both end points of the reactions are calculated and compared to experiment. If adjustments to the intermolecular interactions (i.e., the force field parameters) are required, then they can be carried out for R and P independently. The force fields may include additional functionality (such as multipolar representations of particular fragments) for one state which are not deemed important for the other state. In a second step, ARMD is used to find adiabatic transitions between the two states. To obtain a meaningful overall energetics the constant Δ is calibrated in view of experimental data. EVB is based on a superposition of ionic and covalent resonance forms from which a—typically—small secular matrix is constructed.[13] As such, EVB is rooted in the well established concept of valence bond theory. The resonance forms are mixed through off diagonal (coupling) matrix elements, and the resulting matrix is diagonalized for every conformation. In its original form, the various parametrized terms were fitted to experimental data.[13,53] First, the Hamiltonian is parametrized for a system in the gas phase. By leaving the covalent and off-diagonal terms unchanged and only modifying the ionic terms, a Hamiltonian for the system in a solvent environment is set up. The off-diagonal term couples different states, depends on the solute coordinates, and is typically represented as an exponential or a Gaussian function. The parametrization assumes that the off-diagonal term does not change between the reaction in the gas phase and in solution.[54] In summary, while the two methods are related through the aim to optimally explore the speed force fields to follow reactions in complex environments, the underlying procedures to arrive at such a representation are quite different. It should be noted that in ARMD the R and P side of the reaction are parametrized individually, whereas they are coupled in EVB.

Limitations of ARMD as presented here include processes where the quantum nature (e.g., tunneling, nonadiabaticity, coherence) of the reaction dominates. This is most obviously the case in small molecular systems for which other and potentially more suitable approaches have been developed.[15,16,55] An example from the condensed phase is bond-breaking in MbNO where coherent motion arises from the coupling of the electronic degrees of freedom to the nuclear dynamics during the spin-state change.[56] Experimentally, distinct oscillations with periods of 430 and 150 fs were observed which were related to heme doming and the iron-histidine motion. On the other hand, isomerization reactions or ligand rebinding are examples where coherence is expected to be unimportant. An improvement that will allow to more realistically investigate reactions from ARMD is to introduce a coordinate-dependent asymptotic shift $\Delta(\vec{q})$. Here, $\vec{q}$ describes directions (or progression coordinates) which are found to be important from simulations with a coordinate-independent Δ. Once $\vec{q}$ is known, $\Delta(\vec{q})$ can be obtained from electronic structure calculations.

Other interesting problems that could be treated with ARMD include, for example, (1) adiabatic electron transfer, (2) adiabatic atom transfer, or (3) solid state phase transformations. Concerning (1), the charge transfer band of organic analogs of symmetrical transition-metal-centered intervalence compounds have been investigated experimentally.[57] It was found that for such strongly adiabatic systems classical theory without tunneling correction reproduces the observed rate constants. Mixed-valence isomers for which strong coupling has been found by using infrared spectroscopy[58] and class III intervalence compounds[59,60] are additional candidates for which ARMD may be useful. Other interesting systems in this class include electron transport in hematite[61] (where the interaction between the reactant and product electronic state is 0.20 eV, which is consistent with adiabatic electron transfer) or photoinduced adiabatic electron transfer in strongly coupled dye/semiconductor colloidal systems.[62] Regarding (2), ARMD may be used to study the dynamics and energetics of adiabatic atom transfer reactions such as concerted proton—electron transfer in the oxidation of hydrogen-bonded phenols which have been found to be not highly nonadiabatic.[63] Also, it might be of interest to investigate the dynamics of the decomposition reaction $H_2SO_4 \rightarrow SO_3 + H_2O$. The mechanism involved is high vibrational excitation of the OH stretching motion in the electronic ground state.[64] For solid state phase transition (example (3) above) one typically assumes that transformations follow adiabatic pathways. For such processes, ARMD could be applied in much the same way as for the conformational equilibrium in neuroglobin. In this context it is interesting to note that very recently the role of nonadiabaticity in the iron bcc to hcp phase transformation was investigated. These calculations used a nudged elastic band approach to connect the initial and final states with a predescribed reaction coordinate.[65] More detailed investigations including free nuclear dynamics could give additional insight in the reorganization mechanism and the role of nonadiabaticity for such problems.

ARMD in its current formulation assumes that once the crossing between the two potential energy surfaces is reached, the reaction takes place with probability one. However, there are also cases such as long-range electron transfer[66] and nonadiabatic photochemistry[67] where a more detailed knowledge of the crossing region is necessary, or where (nuclear) quantum effects become important. Such extensions are possible by using a probability

$p < 1$ for switching the surface when a crossing is found or by allowing hops between the potential energy surfaces away from the crossing seam. Their development will provide a natural extension of ARMD and open up new applications for studying reactive events using validated atomistic force fields.

Acknowledgment. We thank Profs. M. Karplus and J. D. Doll and Dr. S. Mishra for discussions. This work is supported by the Schweizerischer Nationalfonds Project 200021-117810.

References

(1) Warshel, A.; Levitt, M. Theoretical studies of enzymic reactions: dielectric, electrostatic and steric stabilization of the carbonium ion in the reaction of lysozyme. *J. Mol. Biol.* **1976**, *103*, 227.

(2) Singh, U.; Kollman, P. A combined ab initio quantum mechanical and molecular mechanical method for carrying out simulations on complex molecular systems: applications to the CH_3Cl+Cl^- exchange reaction and gas phase protonation of polyethers. *J. Comput. Chem.* **1986**, *7*, 718.

(3) Field, M.; Bash, P.; Karplus, M. A combined quantum mechanical and molecular mechanical potential for molecular dynamics simulations. *J. Comput. Chem.* **1990**, *11*, 700.

(4) Bash, P.; Field, M.; Karplus, M. Free energy perturbation method for chemical reactions in the condensed phase: a dynamical approach based on a combined quantum mechanical and molecular mechanical potential. *J. Am. Chem. Soc.* **1987**, *109*, 8092.

(5) Marti, S.; Andres, J.; Moliner, V.; Silla, E.; Tunon, I.; Bertran, J.; Field, M. A hybrid potential reaction path and free energy study of the chorismate mutase reaction. *J. Am. Chem. Soc.* **2001**, *123*, 1709.

(6) Shaik, S.; Kumar, D.; Visser, S.; Altun, A.; Thiel, W. Theoretical Perspective on the Structure and Mechanism of Cytochrome P450 Enzymes. *Chem. Rev.* **2005**, *105*, 2279.

(7) Field, M. Simulating enzyme reactions: Challenges and perspectives. *J. Comput. Chem.* **2002**, *23*, 48.

(8) Stewart, J. Semiempirical Molecular Orbital Theory. In *Reviews in Computational Chemistry;* Lipkowitz, K., Boyd, D., Eds.; John Wiley & Sons, Inc.:1990; *Vol 1.*

(9) Elstner, M. The SCC-DFTB method and its application to biological systems. *Theor. Chem. Acc.* **2006**, *116*, 316.

(10) Mei, H. S.; Tuckerman, M. E.; Sagnella, D. E.; Klein, M. L. Quantum nuclear ab initio molecular dynamics study of water wires. *J. Phys. Chem. B* **1998**, *102*, 10446.

(11) Meuwly, M.; Karplus, M. Simulation of proton transfer along ammonia wires: An "ab initio" and semiempirical density functional comparison of potentials and classical molecular dynamics. *J. Chem. Phys.* **2002**, *116*, 2572.

(12) Sauer, J.; Döbler, J. Gas-phase infrared spectrum of the protonated water dimer: Molecular dynamics simulation and accuracy of the potential energy surface. *Comput. Phys. Commun.* **2005**, *6*, 1706.

(13) Warshel, A.; Weiss, R. An Empirical Valence Bond Approach For Comparing Reactions In Solution and In Enzymes. *J. Am. Chem. Soc.* **1980**, *102*, 6218.

(14) Åqvist, J.; Warshel, A. Simulation of enzyme reactions using valence bond force fields and other hybrid quantum/classical approaches. *Chem. Rev.* **1993**, *93*, 2523.

(15) Tully, J.; Preston, R. Trajectory surface hopping approach to nonadiabatic molecular collisions: the reaction of H^+ with D_2. *J. Chem. Phys.* **1971**, *55*, 562.

(16) Tully, J. Molecular Dynamics with Electronic Transitions. *J. Chem. Phys.* **1990**, *93*, 1061.

(17) Nutt, D. R.; Meuwly, M. Studying reactive processes with classical dynamics: Rebinding dynamics in MbNO. *Biophys. J.* **2006**, *90*, 1191.

(18) Frauenfelder, H.; McMahon, B.; Austin, R.; Chu, K.; Groves, J. The role of structure, energy landscape, dynamics and allostery in the enzymatic function of myoglobin. *Proc. Natl. Acad. Sci. U.S.A.* **2001**, *98*, 2370.

(19) Frauenfelder, H.; McMahon, B. Hydration, slaving and protein function. *Biophys. Chem.* **2002**, *98*, 35.

(20) Gibson, Q. H.; Smith, M. H. *J. Physiol.* **1957**, *136*, P27.

(21) Keyes, M.; Falley, M.; Lumry, R. Studies of Heme Proteins. II. Preparation and Thermodynamic Properties of Sperm Whale Myoglobin. *J. Am. Chem. Soc.* **1971**, *93*, 2035.

(22) Straub, J. E.; Karplus, M. Molecular-Dynamics Study of the Photodissociation of Carbon-Monoxide from Myoglobin - Ligand Dynamics in the 1st 10 ps. *Chem. Phys.* **1991**, *158*, 221.

(23) Traylor, T.; Sharma, V. Why NO? *Biochemistry* **1992**, *31*, 2847.

(24) Snyder, S.; Bredt, D. Biological roles of nitric oxide. *Sci. Am.* **1992**, *266*, 68.

(25) Petrich, J.; Lambry, J.-C.; Kuczera, K.; Karplus, M.; Poyart, C.; Martin, J.-L. Ligand binding and protein relaxation in heme proteins: a room temperature analysis of NO geminate recombination. *Biochemistry* **1991**, *30*, 3975.

(26) Zhu, L.; Sage, J.; Champion, P. Observation Of Coherent Reaction Dynamics In Heme-Proteins. *Science* **1994**, *266*, 629.

(27) Meuwly, M.; Becker, O. M.; Stote, R.; Karplus, M. NO rebinding to myoglobin: a reactive molecular dynamics study. *Biophys. Chem.* **2002**, *98*, 183.

(28) Kim, S.; Jin, G.; Lim, M. Dynamics Of Geminate Recombination of NO with Myoglobin in Aqueous Solution Probed by Femtosecond Mid-IR Spectroscopy. *J. Phys. Chem. B* **2004**, *108*, 20336.

(29) Nutt, D. R.; Karplus, M.; Meuwly, M. Potential energy surface and molecular dynamics of MbNO: Existence of an unsuspected FeON minimum. *J. Phys. Chem. B* **2005**, *109*, 21118.

(30) Ionascu, D.; Gruia, F.; Ye, X.; Yu, A.; Rosca, F.; Beck, C.; Demidov, A.; Olson, J.; Champion, P. Temperature-dependent studies of NO recombination to heme and heme proteins. *J. Am. Chem. Soc.* **2005**, *127*, 16921.

(31) Burmester, T.; Weich, B.; Reinhardt, S.; Hankeln, T. A vertebrate globin expressed in the brain. *Nature* **2000**, *407*, 520.

(32) Sun, Y.; Jin, K.; Peel, A.; Mao, X. O.; Xie, L.; Greenberg, D. Neuroglobin protects the brain from experimental stroke in vivo. *Proc. Natl. Acad. Sci. U.S.A.* **2003**, *100*, 3497.

(33) Vallone, B.; Nienhaus, K.; Brunori, M.; Nienhaus, G. The Structure of Murine Neuroglobin: Novel Pathways for Ligand Migration and Binding. *Proteins* **2004**, *56*, 85.

(34) Du, W.; Syvitski, R.; Dewilde, S.; Moens, L.; La Mar, G. Solution ^{1} H NMR Characterization of Equilibrium Heme Orientational Disorder with Functional Consequences in Mouse Neuroglobin. *J. Am. Chem. Soc.* **2003**, *125*, 8080.

(35) Brooks, B. R.; Bruccoleri, R. E.; Olafson, B. D.; States, D. J.; Swaminathan, S.; Karplus, M. A program for macromolecular energy, minimization and dynamics calculations. *J. Comput. Chem.* **1983**, *4*, 187.

(36) Lee, S.; Warshel, A. A local reaction field method for fast evaluation of long-range electrostatic interactions in molecular simulations. *J. Chem. Phys.* **1992**, *97*, 3100.

(37) Ewald, P. 'Die Berechnung optischer and elektrostatischer Gitterpotentiale′. *Ann. Phys.* **1921**, *369*, 253.

(38) MacKerell, A. D., Jr.; Bashford, D.; Bellott, M.; Dunbrack, R. L., Jr.; Evanseck, J. D.; Field, M. J.; Fischer, S.; Gao, J.; Guo, H.; Ha, S.; Joseph-McCarthy, D.; Kuchnir, L.; Kuczera, K.; Lau, F. T. K.; Mattos, C.; Michnick, S.; Ngo, T.; Nguyen, D. T.; Prodhom, B.; Reiher, W. E., III; Roux, B.; Schlenkrich, M.; Smith, J. C.; Stote, R.; Straub, J. E.; Watanabe, M.; Wiorkiewicz-Kuczera, J.; Yin, D.; Karplus, M. All-atom empirical potential for molecular modeling and dynamics studies of proteins. *J. Phys. Chem. B* **1998**, *102*, 3586.

(39) Jorgensen, W.; Chandrasekhar, J.; Madura, J.; Impey, R.; Klein, M. Comparison of simple potential functionsfor simulating liquid water. *J. Chem. Phys.* **1983**, *79*, 926.

(40) Brooks, C., III; Karplus, M. Deformable stochastic boundaries in molecular dynamics. *J. Chem. Phys.* **1983**, *79*, 6312.

(41) Van Gunsteren, W. F.; Berendsen, H. J. C. *Mol. Phys.* **1977**, *34*, 1311.

(42) Young, R.; Frauenfelder, H.; Johnson, J.; Lamb, D.; Nienhaus, G.; Phillipp, R.; Scholl, R. Time- and temperature dependence of large-scale conformational transitions in myoglobin. *Chem. Phys.* **1991**, *158*, 315.

(43) Zhu, C.; Nangia, S.; Jasper, A.; Truhlar, D. G. Coherent switching with decay of mixing: An Improved treatment of electronic coherence for non-Born-Oppenheimer trajectories. *J. Chem. Phys.* **2004**, *121*, 7658.

(44) Zhu, C.; Jasper, A.; Truhlar, D. G. Non-Born-Oppenheimer trajectories with self-consisting decay of mixing. *J. Chem. Phys.* **2004**, *120*, 5543.

(45) Margulis, C.; Guallar, V.; Sim, E.; Friesner, R.; Berne, B. A New Semiempirical Approach to Study Ground and Excited States of Metal Complexes in Biological Systems. *J. Phys. Chem. B* **2002**, *106*, 8038.

(46) Torrie, G.; Valleau, J. Nonphysical sampling distributions in Monte Carlo free-energy estimation: Umbrella sampling. *J. Comput. Phys.* **1977**, *23*, 187.

(47) Schlitter, J.; Engels, M.; Krüger, A. Targeted molecular dynamics: a new approach for searching pathways of conformational transitions. *J. Mol. Graph.* **1994**, *12*, 84.

(48) Laio, A.; Parinello; M. Escaping free-energy minima. *Proc. Natl. Acad. Sci.* **2002**, *99*, 12562.

(49) Sugita, Y.; Okamoto, Y. Replica-exchange molecular dynamics method for protein folding. *Chem. Phys. Lett.* **1999**, *314*, 141.

(50) Li, H.; Elber, R.; Straub, J. E. Molecular dynamics simulation of NO recombination to myoglobin mutants. *J. Biol. Chem.* **1993**, *268*, 17908.

(51) Northrup, S. H.; Pear, M. R.; Lee, C.-Y.; McCammon, J. A.; Karplus, M. Dynamical theory of activated processes in globular proteins. *Proc. Natl. Acad. Sci. U.S.A.* **1982**, *79*, 4035.

(52) Panchenko, A. R.; Wang, J.; Nienhaus, G. U.; Wolynes, P. G. Analysis of ligand binding to heme proteins using a fluctuating path description. *J. Phys. Chem.* **1995**, *99*, 9278.

(53) Coulson, C. A.; Danielsson, U. Ionic and covalent contributions to the hydrogen bond. 1. *Ark. Fys.* **1954**, *8*, 239.

(54) Hong, G. Y.; Rosta, E.; Warshel, A. Using the constrained DFT approach in generating diabatic surfaces and off diagonal empirical valence bond terms for modeling reactions in condensed phases. *J. Phys. Chem. B* **2006**, *110*, 19570.

(55) Miller, W. H.; George, T. F. Semiclassical Theory of Electronic Transtions in Low-Energy Atomic and Molecular Collisions Involving Several Nuclear Degrees of Freedom. *J. Chem. Phys.* **1972**, *56*, 5637.

(56) Zhu, L.; Sage, J. T.; Champion, P. M. *Science* **1994**, *266*, 629.

(57) Nelsen, S. F.; Ismagilov, R. F.; Trieber, D. A., II. Adiabatic electron transfer: comparison of modified theory with experiment. *Nature* **1997**, *278*, 846.

(58) Londergan, C. H.; Salsman, J. C.; Lear, B. J.; Kubiak, C. P. Observation and dynamics of "mixed-valence isomers" and a thermodynamic estimate of electronic coupling parameters. *Chem. Phys.* **2006**, *324*, 57.

(59) Nielsen, S. F.; Weaver, M. N.; Luo, Y.; Lockard, J. V.; Zink, J. I. Use of the neighboring orbital model for analysis of electronic coupling in Class III intervalence compounds. *Chem. Phys.* **2006**, *324*, 195.

(60) D'Alessandro, D. M.; Keene, F. R. Current trends and future challenges in the experimental, theoretical and computational analysis of intervalence charge transfer (IVCT) transitions. **2006**, *35*, 424.

(61) Rosso, K. M.; Smith, D. M. A.; Dupuis, M. An ab initio model of electron transport in hematite (α-Fe_2O_3 basal planes). *J. Chem. Phys.* **2003**, *118*, 6455.

(62) Huber, R.; Moser, J.-E.; Gratzel, M.; Wachtveitl, J. Real-time observation of photoinduced adiabatic electron transfer in strongly coupled dye/semiconductor colloidal systems with a 6 fs time constant. *J. Phys. Chem. B* **2002**, *106*, 6494.

(63) Rhile, I. J.; Markle, T. F.; Nagao, H.; DiPasquale, A. G.; Lam, O. P.; Lockwood, M. A.; Rotter, K.; Mayer, J. M. Concerted proton-electron transfer in the oxidation of hydrogen-bonded phenols. *J. Am. Chem. Soc.* **2006**, *128*, 6075.

(64) Vaida, V.; Kjaergaard, H. G.; Hintze, P. E.; Donaldson, D. J. Photolysis of sulfuric acid vapor by visible solar radiation. *Science* **2003**, *299*, 1566.

(65) Johnson, D. F.; Carter, E. A. Nonadiabaticity in the iron bcc to hcp phase transformation. *J. Chem. Phys.* **2008**, *128*, 104703.

(66) Marcus, R. Theory of Oxidation-Reduction Reactions Involving Electron Transfer 0.1. *J. Chem. Phys.* **1956**, *24*, 966.

(67) Yarkony, D. Current Issues In Nonadiabatic Chemistry. *J. Phys. Chem.* **1996**, *100*, 18612.

CT800066Q